# 5-Aza-2′-Deoxycytidine Ameliorates Choroidal Neovascularization by Inhibiting the Wnt/β-Catenin Signaling Pathway

Xinyuan Wu,[1] Xi Yang,[1] Xiaochan Dai,[1] Xiuping Chen,[1] Minqian Shen,[1] Jinhui Dai,[1] Fei Yuan,[1] Liyang Wang,[2] Yuanzhi Yuan,[1,3] and Yifan Feng[1]

[1]Department of Ophthalmology, Zhongshan Hospital, Fudan University, Shanghai, China
[2]Department of Ophthalmology, Shanghai Geriatric Medical Center, Shanghai, China
[3]Department of Ophthalmology, Zhongshan Hospital (Xiamen), Fudan University, Xiamen, China

Correspondence: Liyang Wang, Department of Ophthalmology, Shanghai Geriatric Medical Center, No. 2560 Chunshen Road, Minhang District, Shanghai 201100, China; wang.liyang@zs-hospital.sh.cn. Yuanzhi Yuan, Department of Ophthalmology, Zhongshan Hospital (Xiamen), Fudan University, No. 668 Jinhu Road, Xiamen 361000, China; yuan.yuanzhi@zs-hospital.sh.cn. Yifan Feng, Department of Ophthalmology, Zhongshan Hospital, Fudan University, No. 180 Fenglin Road, Shanghai 200032, China; wzafengyifan@163.com.

XW, XY, and XD contributed equally to the work presented here and should therefore be regarded as equivalent authors.

**Received:** August 28, 2023
**Accepted:** January 28, 2024
**Published:** February 12, 2024

Citation: Wu X, Yang X, Dai X, et al. 5-Aza-2′-deoxycytidine ameliorates choroidal neovascularization by inhibiting the Wnt/β-catenin signaling pathway. *Invest Ophthalmol Vis Sci.* 2024;65(2):23. https://doi.org/10.1167/iovs.65.2.23

**Purpose.** Choroidal neovascularization (CNV) can constitute the final pathology of many ocular diseases and result in severe vision loss. Studies have demonstrated that DNA methylation is critical in retinal development, aging, and disorders. The current work investigated the effects and underlying mechanism of 5-Aza-2′-deoxycytidine (5-aza-dC), a suppressor of DNA methylation, in the pathological progression of CNV.

**Methods.** The DNA methylation profiles of retinal pigment epithelial (RPE)/choroidal complexes in normal and laser-induced CNV mice were assessed by Arraystar Mouse RefSeq Promoter Arrays. The CNV area and blood flow density and intensity were observed by optical coherence tomography angiography, and fluorescence leakage was examined by fundus fluorescein angiography in CNV mice with systemic administration of 5-aza-dC. The effects of 5-aza-dC on the biological functions of bEnd.3 cells were estimated by related assays. *Notum* gene promoter methylation was measured using bisulfite sequencing PCR. Methyltransferases and Wnt signaling-related genes were detected in animal and cell culture experiments by real-time PCR and immunoblot.

**Results.** Methyltransferases were upregulated, but Notum (a secretion inhibitor of Wnt signaling) was downregulated in the RPE/choroidal complexes of mice with experimental CNV. Intraperitoneal injection of 5-aza-dC inactivated the Wnt pathway and ameliorated the lesion area and the intensity and density of blood flow, as well as the degree of leakage in CNV. In vitro, vascular endothelial growth factor A (VEGFA) stimulation promoted methyltransferases expression and suppressed Notum expression, consequently activating Wnt signaling, whereas exogenous 5-aza-dC reversed VEGFA-induced hyperpermeability, proliferation, migration, and tube formation in bEnd.3 cells via demethylation of Notum promoter.

**Conclusions.** We observed that 5-aza-dC attenuates the growth of CNV by inhibiting the Wnt signaling pathway via promoter demethylation of the Wnt antagonist Notum. These findings provide a theoretical basis for methylation-based treatment with the Notum gene as a potential target for CNV treatment.

Keywords: DNA methylation, Wnt signaling pathway, 5-aza-dC, notum, choroidal neovascularization

Choroidal neovascularization (CNV) is characterized by immature blood vessels that invade the subretinal space, jointly increasing the occurrence of exudation and hemorrhage, which can serve as the final pathology of many eye disorders such as age-related macular degeneration (AMD) and pathologic myopia.[1,2] Mounting evidence suggests that vascular endothelial growth factor (VEGF) is a major driver of angiogenesis in CNV pathogenesis; therefore, intravitreal anti-VEGF treatment is considered a first-line treatment option for CNV.[3–5] However, only 30% to 35% of people show improved vision following treatment with anti-VEGF therapies, highlighting that pathogenic pathways other than VEGF contribute to CNV.[6,7] Also, long-term anti-VEGF drug injection has been associated with neurotoxicity, chorioretinal/retinal atrophy, and other potential risks such as endophthalmitis, retinal detachment, and uveitis.[8,9] Therefore, exploring novel mechanisms of CNV and identifying new molecular targets to improve therapeutic responses are very urgent and necessary.

DNA methylation is an epigenetic alteration that regulates genes without modifying their sequences, which usually occurs on the cytosine of 5′-CpG-3′dinucleotide (CpG island) in the genome. A methyl group is transferred by *S*-adenosylmethionine with the mediation of DNA methyltransferases (DNMTs) to generate 5-methylcytosine. When CpG islands in the DNA promoter box are methylated,

their binding to transcription factors is likely to be altered, resulting in the silencing of downstream genes.[10,11] Several studies have demonstrated that DNA methylation is critical with regard to retinal development, aging, and disease, especially AMD and diabetic retinopathy.[12–14] However, how DNA methylation affects CNV development and its specific mechanisms have not been fully clarified.

As a nonselective DNMT suppressor, 5-Aza-2′-deoxy cytidine (5-aza-dC) exerts protective effects in many pathological conditions.[15–17] Administration of 5-aza-dC is known to inhibit antioxidant enzyme expression in both human retinal endothelial cells (HRECs) and rat retinal tissues, thus protecting them from oxidative stress–related injuries under diabetic conditions.[18] Demethylation with 5-aza-dC also decreases VEGF/pigment epithelium–derived factor (PEDF) ratio and ameliorates the adverse effects of diabetic stimuli (e.g., high glucose, interleukin-1$\beta$) in HRECs and human retinal pigment epithelial (HRPE) cells.[19] 5-aza-dC could significantly suppress transforming growth factor-beta (TGF-$\beta$)-induced HRPE cell transdifferentiation, playing an important role in the pathogenesis of proliferative vitreoretinopathy.[20] Moreover, a recent study demonstrated that treatment with 5-aza-dC mitigated VEGF expression in transmitochondrial AMD cybrid cells in vitro, suggesting that this drug might be useful in inhibiting neovascularization in the late stage of AMD.[21]

Here, Arraystar Mouse RefSeq Promoter Arrays (Arraystar, Inc., Rockville, MD, USA) were utilized to examine DNA methylation in the whole genome in RPE/choroidal tissues from laser-induced CNV mice versus normal controls. In addition, the effects of 5-aza-dC on biological functions in endothelial cells (ECs) under high VEGF conditions and the growth of CNV following laser irradiation in mice were examined to assess their value as novel treatment options for CNV. We showed that DNA methylation is important for the development of CNV, providing the basis for further studies.

## Methods

### Reagents

The 5-aza-dC (a nonselective DNMT inhibitor) and LP-922056 (a selective Notum pectinacetylesterase inhibitor) were purchased from Merck KGaA (Darmstadt, Germany) and dissolved in dimethylsulfoxide (DMSO) at 25 mg/mL and 2 mg/mL concentrations, respectively. The mouse recombinant proteins of vascular endothelial growth factor A (VEGFA), Wnt-3a, and Notum were obtained from R&D Systems (Minneapolis, MN, USA) and resuspended in sterile phosphate-buffered saline (PBS) containing at least 0.1% bovine serum albumin (BSA) at recommended concentrations. All of these solutions were aliquoted and kept at −20°C or −80°C until use.

### Animals

C57BL/6J mice (6–8 weeks old) provided by SLAC Laboratory Animal (Shanghai, China) were maintained at 23°C to 25°C and 50% to 60% humidity with a 12-hour photoperiod. The animal study was approved by the Ethics Committee on Animal Experiments of Animal Care Committee of Fudan University (No. 2019-285), and followed the ARVO Statement for the Use of Animals in Ophthalmic and Vision Research. A 1-week animal acclimatization was performed prior to experimentation.

### Laser-Induced CNV Model Establishment and Treatment

CNV model induction and assessment were performed by laser photocoagulation.[22,23] In brief, mice were anesthetized with 2% sodium pentobarbital (30 mg/kg; Sigma-Aldrich, St. Louis, MO, USA), followed by bilateral pupil dilation using 1% tropicamide (Alcon Laboratories, Ft. Worth, TX, USA). Laser photocoagulation (VISULAS 532s; Carl Zeiss Meditec, Jena, Germany) was performed bilaterally with the following parameters: spot size, 100 µm; duration, 100 ms; and power, 120 mW. Eight laser spots were applied around the optic nerve in each eye by using a coverslip as a contact lens. All laser burns had the appearance of a cavitation bubble, and the spots that contained hemorrhage or failed to develop a bubble were excluded from the analysis. Mice were randomized to three groups: normal control with no treatment; CNV+DMSO (mice were administered laser irradiation followed by daily injections of 0.1 mL DMSO); and CNV+5-AZA (mice were administered laser irradiation followed by daily injections of 5-aza-dC at a dose of 1 mg/kg). After evaluation of the area and leakage of CNV lesions by optical coherence tomography angiography (OCTA) and fundus fluorescein angiography (FFA) on day 7, euthanasia was performed by intraperitoneally injecting an overdose of 2% sodium pentobarbital (200 mg/kg), and the eyes were enucleated for quantitative real-time polymerase chain reaction (qRT-PCR), western blot analysis, and immunofluorescence staining as described below.

### DNA Extraction and MeDIP- ChIP Analysis

The methylation status of global DNA of individual samples was determined by Methyl-DNA immunoprecipitation-chip (MeDIP-ChIP), according to the manufacturer's guideline detailed in the NimbleGen MeDIP-ChIP protocol (Nimblegen Systems, Inc., Madison, WI, USA). Genomic DNA (gDNA) extraction was conducted by employing the DNeasy Blood & Tissue Kit (QIAGEN, Hilden, Germany). A NanoDrop ND-1000 spectrophotometer (Thermo Fisher Scientific, Waltham, MA, USA) was utilized for gDNA quantitation and quality assessment. Then, sonication was performed to yield 200-bp to 1000-bp fragments. Immunoprecipitation of methylated DNA was carried out with BioMag magnetic beads (Bangs Laboratories, Fishers, IN, USA) coupled with anti-5-methylcytidine mouse monoclonal antibody. The immunoprecipitated DNA underwent purification using phenol chloroform extraction and ethanol precipitation. The total input and immunoprecipitated DNAs were linked to Cy3- and Cy5-conjugated random 9-mers, respectively, followed by hybridization to the Arraystar Mouse 4×180 K RefSeq Promoter Array, which contains 22,327 known RefSeq promoter regions (–1300 bp to +500 bp of the transcription start sites) entirely covered by ~180,000 probes with approximately 205-bp spacing. An Agilent G2505 C Microarray Scanner System (Agilent Technologies, Rockville, MD, USA) was utilized for scanning.

### Microarray Data Analysis

Raw data extraction to generate pair files employed NimbleScan (Roche NimbleGen, Pleasanton, CA, USA). Median-centering quantile normalization and linear smoothing were performed utilizing the Ringo, limma, and MEDME packages. Then, a normalized log2-ratio value (*_ratio.gff

Investigative Ophthalmology & Visual Science

file) was generated for every sample, from which enriched peaks (sliding window width, 1500 bp; mini probes/peak, 2; *P* value minimum cutoff ($-\log_{10}$), 2; maximum length between neighboring probes in a peak, 500 bp) were identified with NimbleScan 2.5 (Roche NimbleGen). Upon obtaining *_peaks.gff files, the determined peaks were mapped to transcripts and CpG islands. Differentially enriched peaks (DEPs) were determined by the M' method, which reveals substantial gene changes. Next, $\log_2$ ratios for all probes in the DEP region were utilized to carry out a cluster analysis to directly reveal the methylation of DEP probes in various samples. Genes with DEPs in their promoters were considered differentially methylated genes (DMGs) and underwent Kyoto Encyclopedia of Genes and Genomes (KEGG) pathway and Gene Ontology (GO) analyses. The promoters were classified into high (HCP), intermediate (ICP), and low (LCP) CpG promoters/regions, with high, intermediate, and low CpG density promoters, respectively.

## Optical Coherence Tomography Angiography

Ultra-widefield swept-source OCTA (BMizar; TowardPi Medical Technology, Beijing, China) was performed at 7 days following the initial laser treatment. Anesthetized mice were placed on a platform in front of the camera lens, with a polymethyl methacrylate contact lens (diameter, 3.2 mm; corneal surface, R 1.7 mm; outer surface, R 1.8 mm; central thickness, 0.3 mm; Heidelberg Engineering; Heidelberg, Germany) on each eye during OCTA imaging to prevent corneal dehydration and cataract formation. Images of 24 × 20-mm2 areas were obtained for all eyes with a standardized focus setting of +24.00 diopters; accordingly, the mode of the OCTA reference arm was adjusted to the animal eye in the imaging system. Image analysis was performed by a previously established approach.[24,25] Two blinded graders (FY, XW) independently drew the outlines of CNV lesions; then, the results were compared and correlation coefficients were calculated. The area of the CNV lesion and blood flow were quantified by the automated measuring tool provided by the system's manufacturer (TowardPi). After selecting each laser spot manually, the system would automatically determine the radius and area of the selected circle and the included blood flow area. The laser-determined lesion size was averaged for all examined mice, and then the blood flow area was divided by the area of laser lesion to obtain the density of blood flow. ImageJ (National Institutes of Health, Bethesda, MD, USA) was used to determine the blood flow signal pixel intensity of the B-scan in the region where the laser spot was located.

## Fundus Fluorescein Angiography

Seven days after laser treatment, FFA was performed to observe CNV leakage. Following anesthesia and pupil dilation using a 0.5% tropicamide–phenylephrine ophthalmic solution (Mydrin; Santen Pharmaceutical, Osaka, Japan), intraperitoneal injection of fluorescein sodium (Fluorescite, 0.1 mL/kg; Alcon, Geneva, Switzerland) was performed for each mouse. The ocular fundus was consecutively examined with a digital fundus camera (Heidelberg Retina Angiograph). Fluorescein angiograms were blindly and independently evaluated by two assessors (FY, XW) according to previously established criteria; they assigned scores of 0 to 3,[26] where 0 indicated no leakage, faint hyperfluorescence, or mottled fluorescence without leakage; 1, hyperfluorescent lesion with no progressive increase in size or intensity; 2, hyperfuorescence increasing in intensity but not in size with no definite leakage; and 3, hyperfluorescence increasing in intensity and size with definite leakage.

## Cell Culture and Treatment

The bEnd.3 cells (immortalized murine cerebral vascular endothelial cells), provided by American Type Culture Collection (CRL-2299; Manassas, VA, USA), underwent culture in DMEM (KeyGEN BioTECH, Jiangsu, China) containing 450 mg/dL glucose and 10% fetal calf serum (FCS; KeyGEN BioTECH), together with 80 U/mL penicillin and 0.08 mg/mL streptomycin at 37°C in a humid atmosphere with 5% $CO_2$. For permeability assays, the subconfluent cells were incubated with 10 ng/mL recombinant mouse VEGFA protein or 200 ng/mL recombinant mouse Wnt-3a protein with or without the presence of 50 ng/mL 5-aza-dC for 48 hours. Moreover, in order to detect the effects of Notum on downstream targets of the Wnt/$\beta$-catenin pathway, bEnd.3 cells were stimulated with 500 ng/mL recombinant mouse Notum protein for 24 hours, and Notum inhibition was evaluated by addition of 1 µM LP-922056.

## Cell Viability Assay

bEnd.3 cell proliferation was measured with a Cell Counting Kit-8 (CCK-8) assay (Beyotime, Shanghai, China) as directed by the manufacturer. bEnd.3 cells in different groups (1000 cells/well) were seeded into 96-well plates. After 24, 48, and 72 hours of treatment, 10 µL of the CCK-8 reagent was supplemented per well, followed by another 2-hour incubation. Absorbance readings at 450 nm were carried out with a FlexStation 3 Multi-Mode Microplate Reader (Molecular Devices, San Jose, CA, USA). Three independent experiments were performed.

## Scratch Migration Assay

The migratory function of bEnd.3 cells was examined by a scratch migration assay.[27] After 6 hours of serum starvation, confluent cells in a six-well plate were scratched with a 200-µL sterile pipette tip. Cellular debris was carefully removed by washing with 1× PBS, and the wounded monolayer was allowed to heal for 48 hours with fresh medium comprised of 2% FCS. At 0, 24, and 48 hours, imaging was performed with an ortho microscope (Olympus, Tokyo, Japan), and ImageJ was utilized for data analysis. Four independent experiments were performed.

## Tube Formation Assay

This assay was performed as previously described.[23] In brief, $10^4$ cells in the supernatant from a given pretreatment were seeded per well in Matrigel-coated 96-well plates. Following an 8-hour incubation, five randomly selected fields were imaged per sample, and the experiment was repeated four times. Image Pro-Plus (IPP) 6.0 (Media Cybernetic, Rockville, MD, USA) was employed for analysis.

## Sodium Fluorescence Assay

Sodium fluorescein salt (FITC-Na; Sigma-Aldrich) was employed for permeability assays in bEnd.3 cells as described in a previous report.[28] Briefly, confluent bEnd.3 cells with indicated treatment in the apical chambers of

Investigative Ophthalmology & Visual Science

Transwell inserts were incubated with fluorescein solution (1 mg/mL) in DMEM without FCS for 1 hour. Collected samples were loaded onto a 96-well plate, and fluorescence intensities in the apical and basal compartments were assessed using a microplate reader, with excitation and emission at 460 and 515 nm, respectively. Diffusion rates were obtained as reported previously.[29] Five independent experiments were performed.

### Transendothelial Electrical Resistance

Transendothelial electrical resistance (TEER) of bEnd.3 cells was obtained with an EVOM2 volt/ohm meter and STX electrodes (World Precision Instruments, Sarasota, FL, USA). In brief, cells were plated in the upper compartment of a Transwell system to confluency. After a 48-hour treatment as described above, TEER was assessed for each of the three wells of the insert, using cell-free wells as background. The final TEER value was determined as TEER ($ohm/cm^2$) = [(Average of 3 measurements/well) − (Background TEER)] × (Area of the insert). Five independent experiments were performed.

### DNMT Activity Assay

Overall DNMT activity was determined with EpiQuik DNMT Activity/Inhibition ELISA Easy Kit (EpigenTek, Farmingdale, NY, USA) per the manufacturer's instructions. Nuclear extracts from the bEnd.3 cells were obtained with the EpigenTek EpiQuik Nuclear Extraction Kit. An Epoch 2 microplate reader (BioTek, Winooski, VT, USA) was utilized for absorbance reading at 450 nm with background reading at 655 nm. Four independent experiments were performed.

### Quantitative Real-Time PCR

Mouse RPE/choroidal complexes from six eyes were pooled as one sample, and three samples were used in each group. Total RNA isolation from bEnd.3 cells or RPE/choroidal samples used TRIzol reagent (Invitrogen, Carlsbad, CA, USA). Reverse transcription employed Hieff PCR Master Mix (Yeasen, Shanghai, China). A PRISM 7500 Fast Real-Time PCR System (Applied Biosystems, Waltham, MA, USA) was employed for qRT-PCR utilizing Hieff UNICON Power qPCR SYBR Green Master Mix (Yeasen) as directed by the manufacturer. Data were normalized to $\beta$-actin expression. The primers utilized are provided in Supplementary Table S1.

### Western Blot Analysis

Mouse RPE/choroidal complexes from six eyes were pooled as one sample, and three samples were used in each group. Total protein extraction from bEnd.3 cells or RPE/choroidal samples employed radioimmunoprecipitation assay lysis buffer (Beyotime) that contained phenylmethylsulphonyl fluoride. The BCA Protein Assay Kit (Beyotime) was utilized for protein quantitation. Equal quantities of total protein were resolved by 10% SDS-PAGE, followed by electrotransfer onto a polyvinylidene fluoride membrane (MilliporeSigma, Bedford, MA, USA). After a 2-hour blocking utilizing 5% skim milk in Tris-buffered saline with 0.05% Tween 20 (TBST; Sangon Biotech, Shanhai, China) at ambient conditions, overnight incubation was carried out with primary antibodies against Notum (ab106448; Abcam, Cambridge, UK), $\beta$-catenin (ab32572; Abcam), non-phospho(active) $\beta$-catenin (ab305261; Abcam), VEGFA (ab46154; Abcam), DNMT1 (5032; Cell Signaling Technology, Danvers, MA, USA), DNMT3A (3598; Cell Signaling Technology), DNMT3B (48488; Cell Signaling Technology), and $\beta$-actin (13E5; Cell Signaling Technology). Next, secondary antibodies (7074 and 7076; Cell Signaling Technology) were added under ambient conditions for 1 hour. An enhanced chemiluminescence (ECL) kit (Thermo Fisher Scientific) was employed for development. ImageJ was utilized for densitometric analysis, with $\beta$-actin as a reference protein.

### Bisulfite Sequencing PCR

Notum promoter (–3000 bp to +100 bp) retrieval used the Transcriptional Regulator Element Database. Upon searching CpG islands in the UCSC Genome Browser, the CpG island in the promoter at –1877 bp to –2000 bp was assessed for methylation status by bisulfite sequencing PCR (BSP). DNA extraction from bEnd.3 cells utilized a Genomic DNA Extraction Kit (Takara Bio, Shiga, Japan). The QIAGEN EpiTect Bisulfate Kit was employed for bisulfate conversion of DNA, as directed by the manufacturer, followed by nested PCR. Primers designed by MethPrimer (http://www.urogene.org/methprimer/; Supplementary Table S1) were employed for BSP. PCR used the following program: 95°C for 3 minutes; 30 cycles at 94°C (30 seconds), 55°C (30 seconds); 72°C (30 seconds); and 72°C (10 minutes). A different primer was applied in the second PCR, using the above steps. Then, PCR products were ligated to the pMD-19T vector (Takara Bio) for sequencing. The methylation status was obtained by counting methylated CpG islands in all clones, and data were provided as a percentage.

### Immunofluorescence Staining

The bEnd.3 cells were incubated for 48 hours with respective media in 24-well plates on L-lysine–coated coverslips and underwent a 20-minute fixation with 4% paraformaldehyde. Permeabilization (5 minutes) was performed using 0.1% Triton X-100 (Sigma-Aldrich), followed by a 1-hour blocking with 1% BSA and overnight incubation with primary antibodies targeting zonula occludens-1 (ZO-1; ab96587; Abcam) at 4°C. Next, Invitrogen Alexa Fluor 488–linked anti-rabbit IgG secondary antibodies (A-11008; Thermo Fisher Scientific) were added for 1 hour under ambient conditions, followed by counterstaining with 4′,6-diamidino-2-phenylindole (DAPI; Sigma-Aldrich). Imaging was carried out with an Olympus BX63 fluorescence microscope.

For tissue slice analysis, Tissue-Tek optimal cutting temperature (O.C.T.) compound (Sakura Finetek, Torrance, CA, USA) was utilized for embedding eyecups, which was followed by sectioning at 10 µm. The samples were blocked with PBS containing 10% normal goat serum, 1% BSA and 0.1% Triton X-100 for 1 hour under ambient conditions. Next, successive incubations were performed with monoclonal antibodies targeting Notum (ab106448; Abcam) at 4°C overnight, and appropriate Invitrogen Alexa Fluor 488–linked secondary antibodies (A-11008; Thermo Fisher Scientific) were added for 2 hours under ambient conditions protected from light. Following three additional PBS washes, sections were counterstained with DAPI and imaged using an Olympus fluorescence microscope.

### Bioinformatics Analysis

Bulk RNA sequencing of retinas and RPE/choroids in dataset GSE135092 was acquired from the Gene Expression Omnibus (GEO) database (https://www.ncbi.nlm.nih.gov/geo), containing 99 donor eyes that had no history of ocular diseases and 23 donors that were previously diagnosed with advanced AMD.[30] The voom/limma package for R (R Foundation for Statistical Computing, Vienna, Austria)[31,32] was utilized, and the differential expressions of mRNAs were visualized with the ggplot2 of R. Moreover, single-cell transcriptomic data from 12 human donor choroids (10 healthy samples and two neovascular AMD samples) and graphs of choroid endothelial cells were acquired from the Spectacle website[33] (https://singlecell-eye.org/app/spectacle/) based on the Voigt et al.[34] dataset. The genes with adjusted $P < 0.05$ were considered to be differentially expressed genes.

### Statistical Analysis

Prism 9.4.0 (GraphPad, Boston, MA, USA) and SPSS Statistics 26.0 (IBM, Chicago, IL, USA) were utilized to analyze data presented as mean ± standard error of the mean (SEM). Two-way ANOVA or unpaired two-sample Student's *t*-test was carried out for comparisons. Multiple group comparisons utilized one-way ANOVA, with post hoc Bonferroni test; $\chi^2$ tests were used to compare categorical data. $P < 0.05$ was deemed to reflect statistical significance.

## Results

### Alterations of DNA Methylation in the Laser-Induced CNV Model

As DNA methylation involves the DNMT family, we first determined which subfamily members mediate the altered patterns of DNA methylation during CNV. DNMT1, DNMT3A, and DNMT3B mRNA amounts were measured by qRT-PCR at 7 days post-laser photocoagulation. All DNMTs showed significantly elevated expression in CNV mice in comparison with control animals (Figs. 1A–1C). To further examine whether laser injury induces abnormal methylation changes in the DNA promoter regions, Arraystar Mouse RefSeq Promoter Arrays were utilized to identify differentially methylated regions in DNA samples that were extracted from control and CNV mice on day 7. The clustering diagram directly shows the methylation of DEP probes in various samples (Supplementary Fig. S1A). In total, 1581 differentially methylated fragments in DNA promoter regions (i.e., 1094 hyper methylated and 487 hypomethylated fragments) were found in CNV mice (Supplementary Fig. S1B). The detected hypermethylated fragments included 750 HCP (68.56%), 216 ICP (19.74%), and 128 LCP (11.70%). The hypomethylated fragments included 192 HCP (39.42%), 129 ICP (26.49%), and 166 LCP (34.09%) (Supplementary Fig. S1C). Collectively, these data suggest that DNA methylation is altered during CNV.

### Downregulation of Notum Expression in Laser-Induced CNV Model

Because methylated cytosines are important in gene silencing efficiency,[35,36] we next focused on the DMGs associated with high CpG-density promoters (Fig. 1D). KEGG pathway analysis showed that hypermethylation of Wnt signaling-related genes was enriched in the CNV group (Fig. 1E; Supplementary Figs. S2A, S2B). Previous studies have indicated that Wnt pathway activation plays a pathogenic role in laser-induced CNV models.[37,38] Therefore, the expression levels of key Wnt signaling-related genes, including *Notum*, *Lrp6*, *Fzd3*, and *Fzd7*, were further verified by qRT-PCR. Unexpectedly, *Notum*, unlike the other three genes, was dramatically decreased in the CNV group compared with the normal group (Figs. 1F–1I). Additionally, GO analysis demonstrated that the *Notum* gene, which matched to catalytic activity in molecular function, had a higher degree of methylation in the CNV mice versus the normal group (Supplementary Figs. S2C, S2D). Recently, *Notum* was described as an extracellular carboxylesterase cleaving the palmitoleate moiety of Wnt proteins, thus inactivating the Wnt pathway.[39,40] As expected, the mRNA levels of downstream targets of the Wnt/$\beta$-catenin pathway, including axis inhibition protein 2 (AXIN2), cyclin D1 (CCND1), and lymphoid enhancer-binding factor-1 (LEF1), were increased markedly in the CNV group (Figs. 1J–1L). Furthermore, results above were verified in public datasets to further demonstrate the expression of DNMTs and Wnt signaling-related genes in human retinas or RPEs/choroids with or without AMD. Analogously, the expression of DNMTs and targets of Wnt signaling pathway in advanced AMD tissue is higher than that in health control tissue. A lower level of *Notum* is expressed in both retinas and RPEs/choroids of advanced AMD, although the difference did not reach statistical significance (Supplementary Figs. S3, S4). Therefore, it is possible that downregulation of the *Notum* gene was involved in the activation of canonical Wnt signaling during CNV formation.

### 5-aza-dC Attenuates VEGFA-Mediated Methylation of *Notum* Promoter in bEnd.3 Cells

To verify that *Notum* promoter hypermethylation causes transcriptional silencing of *Notum* in CNV, the *Notum* promoter region was examined in the bEnd.3 cell line, including the CpG island that encompasses the transcriptional start site, for methylation by the BSP method. bEnd.3 cells were treated with exogenous VEGFA to mimic the pro-angiogenic environment present in CNV. As depicted in Figures 2A to 2D, increased mRNA levels and activities of DNMTs induced by VEGFA were inhibited by pretreatment with the demethylating agent 5-aza-dC. Using the UCSC genome browser, one CpG-rich region was captured within *Notum* (Fig. 2E). A fragment (–2000/–1877) containing 15 CpG sites within the CpG island was amplified for BSP analysis (Fig. 2F). The results showed that exposure to VEGFA for 48 hours significantly increased the methylated CpG sites of the *Notum* promoter region (Fig. 2G), and the number of methylated CpG sites were quantified (Fig. 2H). By contrast, pretreatment with 5-aza-dC could efficiently decrease the methylation ratio (Figs. 2G, 2H). Jointly, the above findings demonstrate that CpG island methylation directly affects epigenetic *Notum* silencing in CNV.

### 5-aza-dC Inhibits Activation of the Wnt Pathway in bEnd.3 Cells

We first detected the impact of *Notum* expression on the downstream targets of the Wnt pathway. *Notum* treatment significantly decreased the mRNA levels of AXIN2, CCND1,

Investigative Ophthalmology & Visual Science

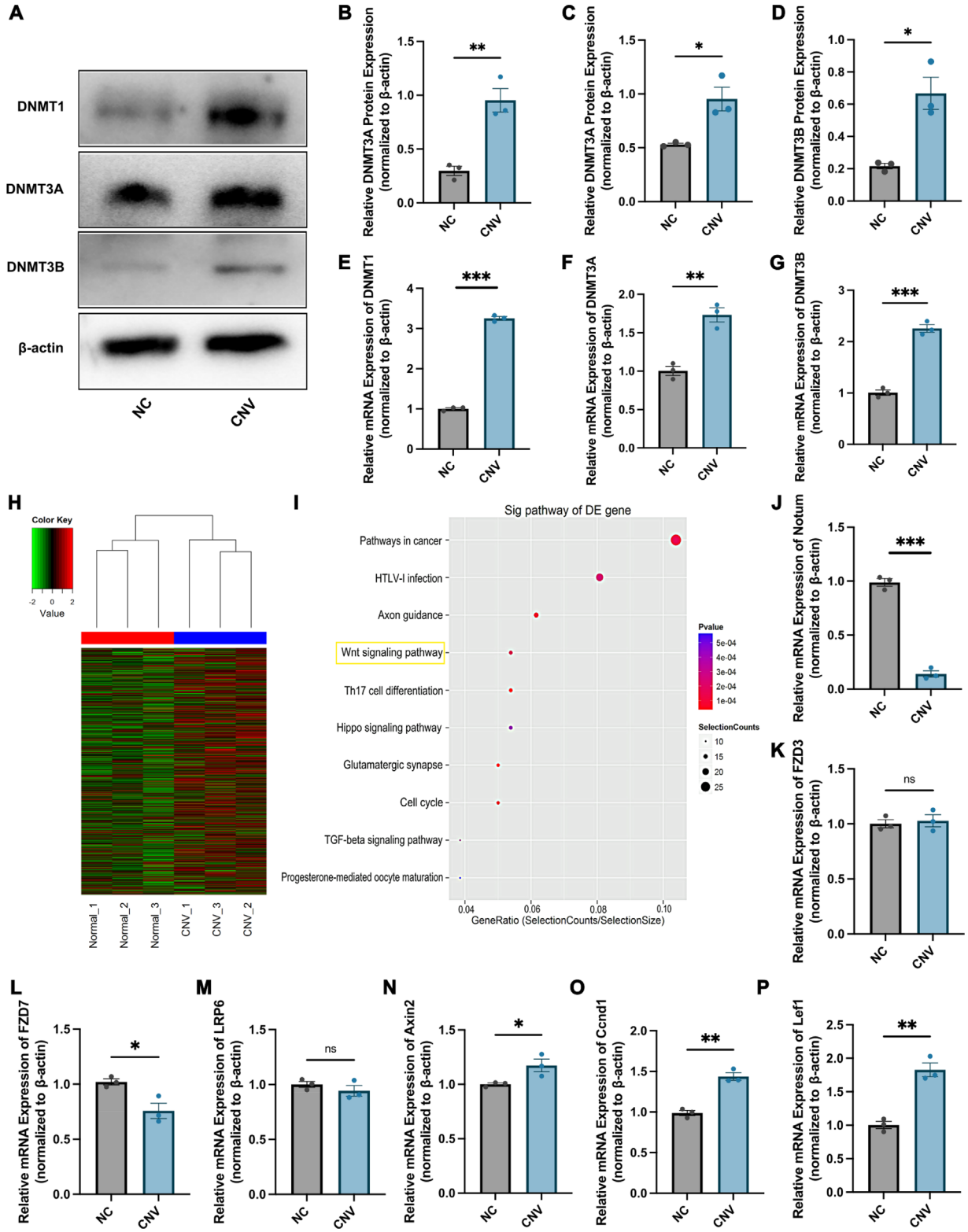


**Figure 1.** Expression of DNMTs and activity of Wnt signaling pathway were increased but *Notum* expression was decreased in laser-induced CNV mice. (**A–D**) Representative western blot and quantitative analysis of DNMT1, DNMT3A, and DNMT3B in REP/choroidal complexes from the indicated groups ($n = 9$ mice/per group for all experiments). (**E–G**) qRT-PCR was performed to detect the mRNA expression of DNMTs in the RPE/choroidal complexes from normal and laser-induced CNV mice ($n = 6$ mice/per group for all experiments). (**H**) Clustering of differentially enriched peaks of methylation in the DNA promoter region in the RPE/choroidal complexes from the normal group and the laser-induced CNV group (*red*, hypermethylation; *green*, hypomethylation). (**I**) Enrichment analysis of KEGG pathways and the top 10 activated pathways identified among hypermethylated differentially methylated genes in the RPE/choroidal complexes from the normal group and the laser-induced CNV group. (**J–P**) qRT-PCR was performed to detect the mRNA expression of Wnt signaling-related genes in the RPE/choroidal complexes from the normal group and the laser-induced CNV group ($n = 9$ mice/per group for all experiments). Each experiment was repeated at least three times, and data in the graphs represent the mean ± SEM. $^{*}P < 0.05$; $^{**}P < 0.01$; $^{***}P < 0.001$.

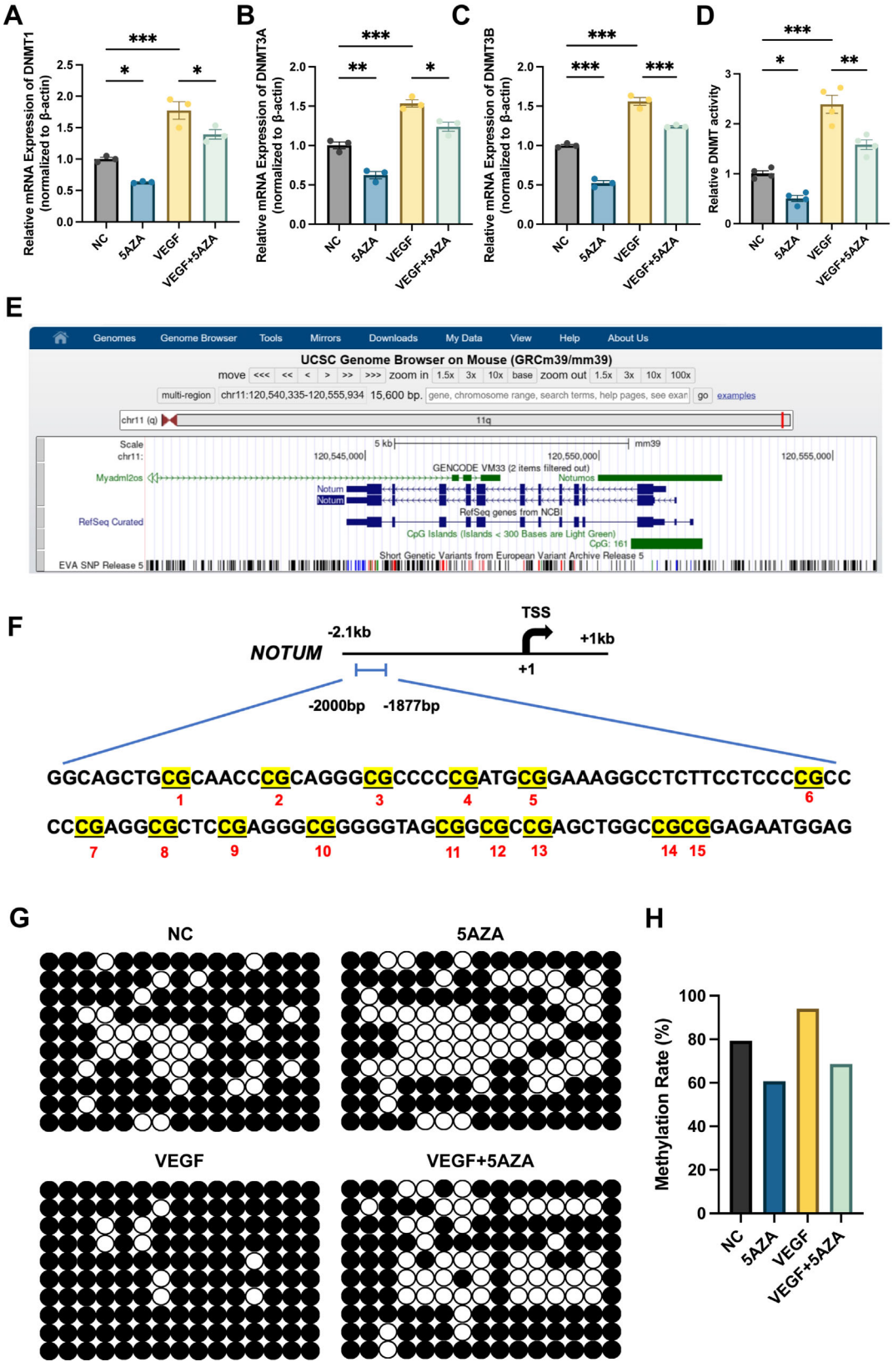


**Figure 2.** 5-aza-dC attenuated VEGFA-mediated methylation of *Notum* promoter in bEnd.3 cells. (**A–C**) qRT-PCR was performed to detect the mRNA expression of DNMTs in the indicated groups. (**D**) ELISA was performed to measure the activity of overall DNMT in the indicated groups. (**E**) Presence of CpG islands across the *Notum* gene as identified using the UCSC Genome Browser. (**F**) Schematic of *Notum* promoter CpG region (–2000 bp to –1877 bp) upstream of the transcriptional start site. (**G**) Bisulfite sequencing PCR of the *Notum* CpG island in bEnd.3 cells after different treatment. Each *horizontal row* represents a single clone; *white circles*, unmethylated CpG dinucleotide; and *black circles*, methylated CpG dinucleotide. (**H**) Percentages indicate the fraction of methylated CpG dinucleotides of the total CpG sites analyzed.

Investigative Ophthalmology & Visual Science

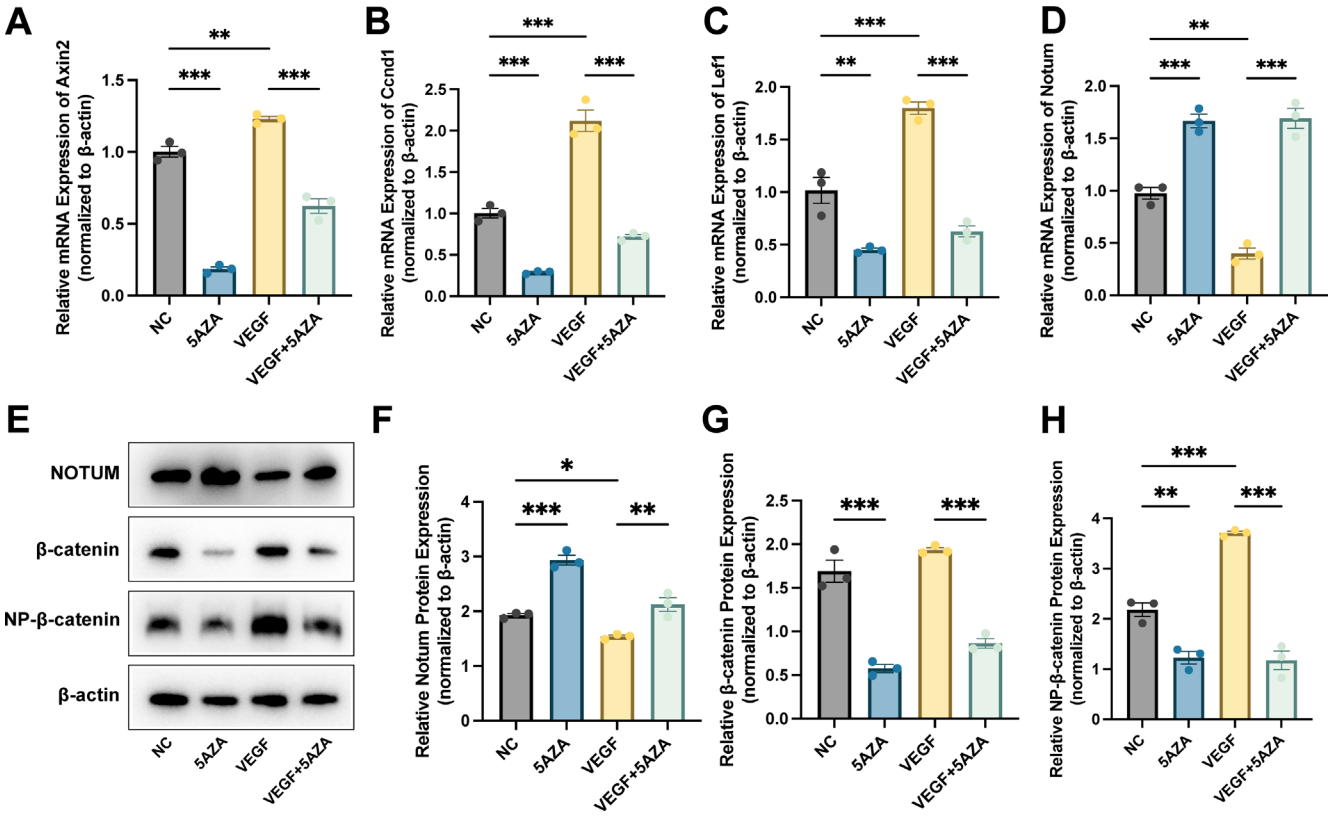


**Figure 3.** 5-aza-dC (5-AZA) reversed the effects of VEGFA on the expression of Wnt signaling-related genes. (**A–D**) qRT-PCR was performed to detect the mRNA expression of Wnt signaling-related genes and *Notum* in the indicated groups. (**E–H**) Representative western blot and quantitative analysis of *Notum*, $\beta$-catenin, and non-phosphorylated $\beta$-catenin (NP-$\beta$-catenin) in the indicated groups. Each experiment was repeated at least three times, and data in the graphs represent the mean ± SEM. $^{*}P < 0.05$; $^{**}P < 0.01$; $^{***}P < 0.001$.

and LEF1 in bEnd.3 cells, and this inhibition effect was restored by LP-922056 (Supplementary Figs. S5A–S5C). A similar pattern was observed for protein expressions of total and non-phosphorylated (activated) $\beta$-catenin (Supplementary Figs. S5D–S5F). Next, we investigated whether 5-aza-dC administration could reduce reduce Wnt signaling activation under different stimuli. In this study, 5-aza-dC substantially reversed the VEGFA- or Wnt3A-induced suppression of *Notum* mRNA expression, and simultaneously, AXIN2, CCND1, and LEF1 mRNA amounts were accordingly decreased in bEnd.3 cells (Figs. 3A–3D; Supplementary Figs. S6A–S6D). In addition, western blot analysis showed that either VEGFA or Wnt3A stimulation reduced the protein levels of *Notum* and elevated the non-phosphorylated $\beta$-catenin levels, and these effects were all reversed by treatment with 5-aza-dC (Figs. 3E–3H; Supplementary Figs. S6F–S6I). Furthermore, VEGFA upregulation in bEnd.3 cells stimulated by Wnt3A suggested a potential positive feedback loop between VEGFA and the Wnt pathway, and this effect was disturbed by 5-aza-dC (Supplementary Figs. S6F, S6J). These results suggest that 5-aza-dC inhibits the Wnt pathway by promoting *Notum* expression in bEnd.3 cells.

## 5-aza-dC Reverses the Biological Function of bEnd.3 Cells

Considering that VEGFA represents a well-established proangiogenic and vascular permeability factor and an important pathogenetic modulator in CNV, we further investigated the effects of 5-aza-dC on the biological function of bEnd.3 cells via VEGFA stimulation. To evaluate the effect of 5-aza-dC on VEGFA-triggered endothelial permeability alteration, the penetration of FITC-Na in the bEnd.3 cell monolayer was assessed by the Transwell system. VEGFA administration markedly enhanced paracellular permeability. Inversely, pretreatment with 5-aza-dC markedly decreased VEGFA-dependent endothelial hyperpermeability with no changes in basal permeability (Fig. 4A). To further examine the effect of 5-aza-dC on the integrity of endothelial tight junctions, ZO-1 localization was assessed by immunofluorescence. As shown in Figure 4B, ZO-1 showed a continuous expression at cell junctions in the control group. VEGFA altered the above distribution pattern to cause a higher discontinuity with lost junctional localization, which was inhibited by 5-aza-dC pretreatment. In control cells, ZO-1 showed an even distribution around the cell–cell junction in bEnd.3 cells. VEGFA administration resulted in fragmented ZO-1 junctions in bEnd.3 cells (Fig. 4B). Furthermore, measurement of TEER, as an indicator of endothelial integrity, in bEnd3 cells in the Transwell system revealed that the VEGFA-induced reduction in TEER was markedly attenuated after 5-aza-dC treatment (Fig. 4C).

Viability, migration, and tube formation in endothelial cells are the critical steps of angiogenesis, which is involved in the pathogenesis of CNV. In the tube formation assay, greater relative tube length was found upon VEGFA

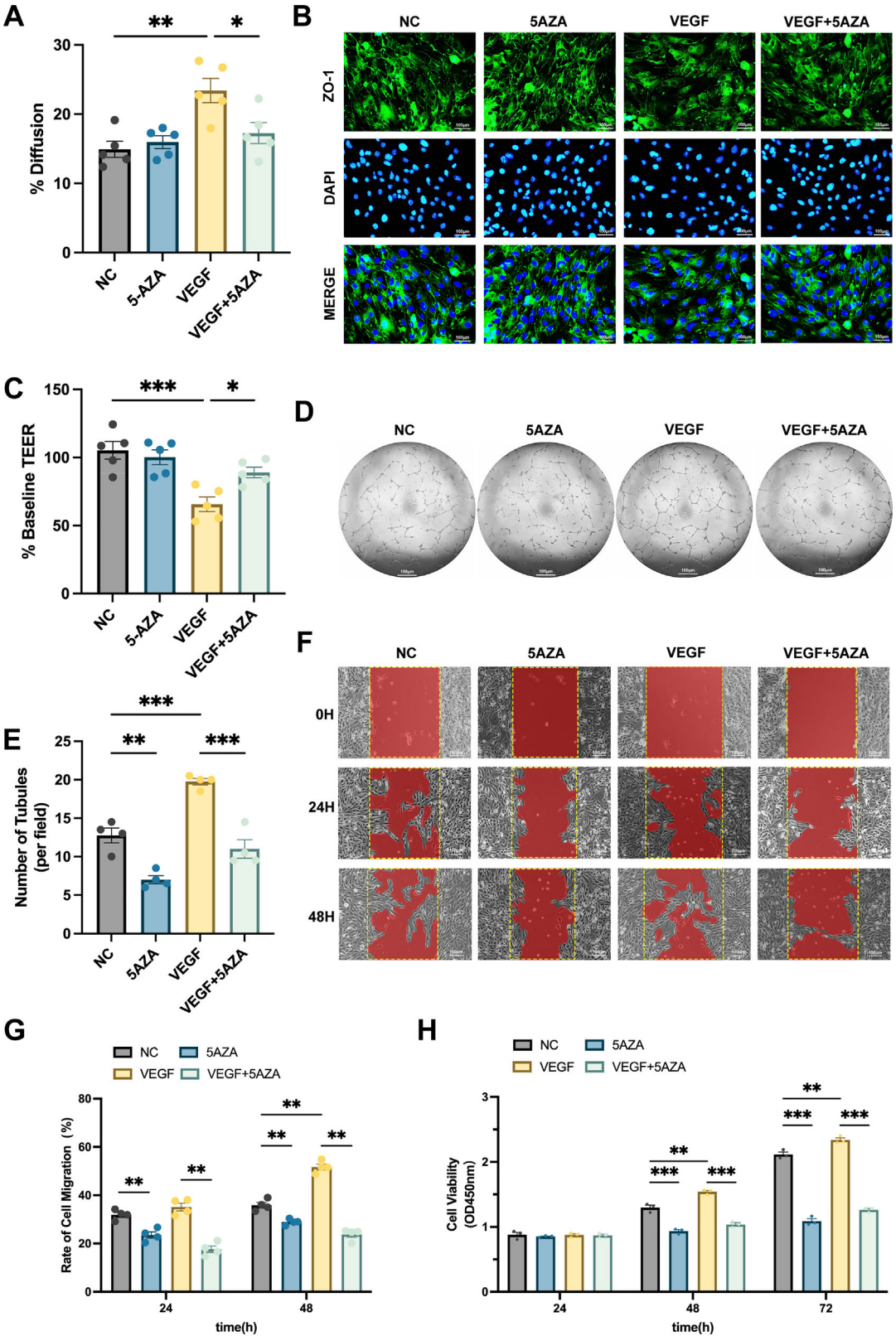


**Figure 4.** 5-aza-dC reversed the biological function of bEnd.3 cells induced by VEGFA. (**A**) FITC-Na leakage and (**C**) TEER of bEnd.3 cells cultured in Transwell membranes at 48 hours after indicated treatments. (**B**) Immunostaining for ZO-1 (*green*) and DAPI (*blue*) in bEnd.3 cells from the indicated groups. *Scale bar*: 100 µm. (**D**, **E**) bEnd.3 cells from the indicated groups were seeded on the Matrigel matrix, and the tube-like structures were quantified at 8 hours after cell seeding. *Scale bar*: 100 µm. (**F**, **G**) Scratch wound assay was performed to assess the migration of bEnd.3 cells from the indicated groups. The percentage of closure areas were quantified and analyzed at 24 hours and 48 hours after cell seeding. *Scale bar*: 100 µm. (**H**) CCK-8 assay was performed to detect the proliferation of bEnd.3 cells from the indicated groups. The absorbance was measured at 450 nm 24, 48, and 72 hours after cell seeding. Each experiment was repeated at least three times, and data in the graphs represent the mean ± SEM. $^{*}P < 0.05$; $^{**}P < 0.01$; $^{***}P < 0.001$.

Investigative Ophthalmology & Visual Science

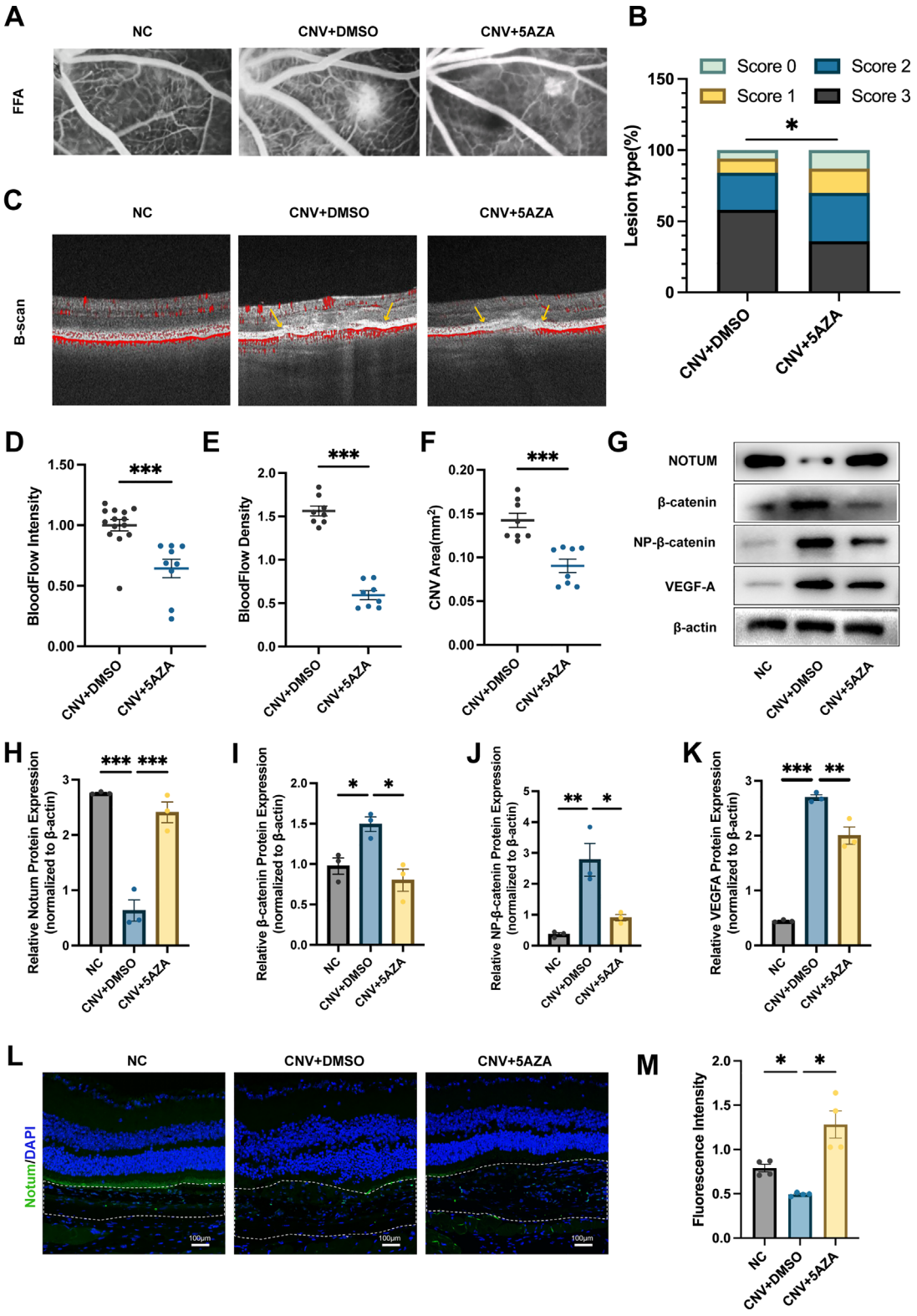


**Figure 5.** Intraperitoneal injection of 5-aza-dC suppressed laser-induced CNV in mice. (**A**, **B**) Representative images of choroidal vascular leakage on FFA from untreated mice or laser-induced CNV mice with intraperitoneal injection of DMSO or 5-aza-dC. Data are expressed as the incidence of CNV angiographic grades of the total laser impacts on each group ($n$ = 8 mice/per group for all experiments). (**C–F**) Representative images of CNV lesions on B-scans with blood flow signals from the indicated groups. CNV lesions are indicated by the *yellow arrows*. CNV area and the intensity and density of blood flow in lesions were compared among each group ($n$ = 8 mice/per group for all experiments). (**G–K**) Representative western blot and quantitative analysis of *Notum*, $\beta$-catenin, non-phospho-$\beta$-catenin (NP-$\beta$-catenin), and VEGFA in REP/choroid complexes from the indicated groups ($n$ = 9 mice/per group for all experiments). (**L**, **M**) Immunofluorescence staining of *Notum* and quantitative analysis of fluorescence intensity from the indicated groups ($n$ = 4 mice/per group for all experiments). Areas designed by *dashed lines* represent RPE/choroidal tissues. *Scale bar*: 100 µm. Each experiment was repeated at least three times, and data in the graphs represent the mean ± SEM. *$P$ < 0.05; **$P$ < 0.01; ***$P$ < 0.001.

stimulation, whereas 5-aza-dC pretreatment decreased the formation of the capillary network (Figs. 4D, 4E). Meanwhile, the migration rates of bEnd.3 cells were elevated after VEGFA treatment for 24 hours and 48 hours, whereas 5-aza-dC pretreatment decreased migration in these cells (Figs. 4F, 4G). Subsequently, the cell viability assay revealed that VEGFA promoted bEnd.3 cell growth, but 5-aza-dC pretreatment reversed the stimulative effects of VEGFA (Fig. 4H). Overall, the above results indicated that 5-aza-dC treatment countered VEGFA-induced angiogenesis and vascular permeability.

### 5-aza-dC Attenuates Progression of Laser-Induced CNV in the Mouse Model

Because of the aberrant DNA methylation in CNV tissues, we hypothesized that alteration of methylation status could inhibit the pathological neovascularization in the context of CNV. To test this hypothesis, we injected the DNA methyltransferase inhibitor 5-aza-dC or vehicle (DMSO) intraperitoneally into mice for 7 consecutive days after laser injury. FFA results showed that the fluorescein leakage of CNV lesions was significantly decreased after 5-aza-dC treatment compared to the CNV plus DMSO group (Figs. 5A, 5B). Consistently, 5-aza-dC treatment also reduced the CNV lesion areas, as well as blood flow intensity and density in CNV lesions, which were quantified by OCTA (Figs. 5C–5F). Moreover, injection of 5-aza-dC resulted in the upregulation of Notum protein expression but downregulation of total and activated/non-phosphorylated $\beta$-catenin expression (Figs. 5G–5J). Additionally, VEGFA protein amounts were also reduced in the CNV model with 5-aza-dC treatment (Figs. 5G, 5K). Furthermore, immunofluorescence staining of cryosections showed that *Notum* was expressed moderately on normal RPE/choroidal layers. At 7 days after laser injury, *Notum* staining was nearly undetectable within CNV lesions in the DMSO group, but 5-aza-dC administration promoted *Notum* expression (Figs. 5L, 5M). Collectively, the above findings suggested that 5-aza-dC may attenuate the CNV formation by inhibiting activation of the Wnt pathway.

## Discussion

Epigenetic changes, including microRNAs, histone modifications, and DNA methylation, are involved in gene expression regulation. DNA methylation can cause long-term gene silencing, and these traits can be inherited.[41] In the eye, DNA methylation is highly involved in retinal development and disorders.[13,14] Differential DNA methylation of several genes, including glutathione S-transferase isoform mu1 (*GSTM1*),[42] age-related macular degeneration susceptibility 2 (*ARMS2*),[43] and lecithin cholesterol acyltransferase (*LCAT*),[44] has been detected in peripheral blood samples from patients with AMD and the control group. Moreover, genome-wide DNA methylation data reported by Porter and colleagues[45] demonstrated differential DNA methylation of SKI proto-oncogene (SKI), transcription-dependent DNA repair mechanisms (GTF2H4), and Tenascin X (TNXB) in human RPE cells obtained from patients with AMD. All of these data indicate that DNA methylation might affect the onset of AMD. However, the characterization of methylation profiles in CNV, which constitutes the late, serious stage of the exudative form of AMD, deserves further investigation. The DNMT inhibitors have been shown to effectively stimulate the reduction of vascularization in a variety of tumor models.[46,47] These previous reports prompted the notion that 5-aza-dC may serve as an inhibitor of pathological CNV, as well. We therefore evaluated the effect of 5-aza-dC on laser-induced CNV using a mouse model and assessed its effect on EC biology in vitro.

In this study, the Arraystar Mouse DNA Promoter Array was utilized to determine methylation profiles in the whole genome in the DNA promoters of the RPE/choroidal complex in mice 7 days after laser photocoagulation because the optimum time point to assess CNV formation is typically at day 7 to day 14. Later, an active healing process begins, and the lesion size decreases.[48] In the current work, we detected >1500 fragments with differential methylation upon laser injury, including 1094 hypermethylated and 487 hypomethylated fragments, suggesting there are widespread methylation alterations during CNV development. Additionally, the mRNA levels and activities of total DNMTs were increased in CNV tissues, corroborating previously reported findings that AMD cases exhibit high total DNMTs activity, in association with DNMT1 and DNMT3B overexpression.[49] Therefore, this work assessed DNMT methylation reversal by 5-aza-dC as a novel treatment option for CNV.

As expected, OCTA showed that CNV size and blood flow intensity and density within the CNV lesion were significantly lower in the 5-aza-dC treatment group than in the DMSO treatment group. FFA also confirmed that choroidal vascular leakage in the CNV area was overtly reduced after 5-aza-dC treatment. Because epigenetic variations are dependent on environmental factors, the effect of 5-aza-dC on endothelial function was examined to confirm that our cell culture model retains the epigenetic features of the original tissue. Accordingly, VEGFA stimulation increased the expression levels and activities of DNMTs in ECs. Pretreatment with 5-aza-dC could reverse VEGFA- or Wnt3A-mediated migration, proliferation, and tube formation ability in ECs. Meanwhile, 5-aza-dC also abolished the aggravated effects of VEGFA or Wnt3A on the disruption of tight junctions and monolayer permeability in ECs. Because the hyperactivity and hyperpermeability of ECs have been implicated in the onset and progression of CNV, the current results point to a possible anti-angiogenic effect of 5-aza-dC. This corroborates previous reports indicating the potential usefulness of 5-aza-dC in vascular disorders.[18,50–52]

Wnt/$\beta$-catenin signaling in mammals is mainly comprised of Wnt signal transduction in the cytoplasmic membrane, regulation of $\beta$-catenin stability in the cytosol, and activation of target genes in the nucleus.[53] Recent evidence demonstrates that Wnt/$\beta$-catenin signaling regulates the functions of endothelial cells and affects angiogenesis in many vascular eye diseases, including AMD.[54–56] For instance, induced Wnt/$\beta$-catenin pathway was reported in both clinical AMD macular tissue specimens and in the mouse laser-induced CNV model.[57] Blocking Wnt/$\beta$-catenin signaling with an anti-LRP6 antibody (Mab2F1) could simultaneously reduce vascular leakage from the CNV lesion and reduce the CNV area.[58] In a previous study, we reported that Wnt/$\beta$-catenin signaling suppression alleviates vascular fibrosis.[59] Together, the above findings suggest that Wnt/$\beta$-catenin signaling activation might play a critical role in CNV pathogenesis. Intriguingly, the *Notum* promoter was methylated and Wnt/$\beta$-

Investigative Ophthalmology & Visual Science

catenin signaling was hyperactivated in laser-induced CNV tissues or VEGFA-stimulated ECs, as demonstrated above. In addition, BSP analysis revealed that VEGFA stimulation increased *Notum* promoter methylation in ECs, which was reversed by pretreatment with 5-aza-dC. *Notum* is a direct target and modulator of the Wnt/$\beta$-catenin pathway and is involved in the negative feedback loop required for weakening the signal strength of Wnt/$\beta$-catenin signaling by encoding an extracellular deacetylase that removes the covalently bound lipid portion of Wnt ligands in the cell membrane.[39,40] Although bioinformatic analysis showed that there was no difference in *Notum* expression between normal and neovascular AMD (nAMD) eyes, a relatively low level of *Notum* in the nAMD group revealed its potential role in CNV development. In combination with the above reports, the present results suggest that downregulation of *Notum* induced by DNA methylation may promote the progression of CNV, an effect realized through the activation of the Wnt pathway.

This study had several limitations. First, DNMTs show ubiquitous expression, beyond ECs. Because CNV is a complex process resulting from dysfunction of multiple cell types (e.g., RPE cells, ECs, immune cells, pericytes, smooth muscle cells), systemic approaches are required to comprehensively examine how global methylation alterations and the crosstalk between various cell types modulate the pathogenetic mechanisms of this disease. Second, no cause-and-effect relationship was demonstrated between DNA hypermethylation and impaired endothelial function in mice with experimental CNV. Finally, a direct protective role for *Notum* in CNV development was not established in the present study. Thus, gain- and loss-of-function experiments with *Notum* should be performed in further studies to identify its role in CNV development.

## Conclusions

To sum up, as shown in Figure 6, we provide evidence that global DNA methylation and DNMT expression are significantly elevated in the laser-induced CNV mouse model and that promoter methylation of the Wnt antagonist *Notum* is involved in VEGFA-induced endothelial cell dysfunction. As a DNMT suppressor, 5-aza-dC could attenuate CNV growth in cell culture and mouse experiments via inactivation of the Wnt pathway. These data provide novel insights into treatment approaches using methylation drugs and reveal the potential for *Notum* to serve as a therapeutic target for CNV.

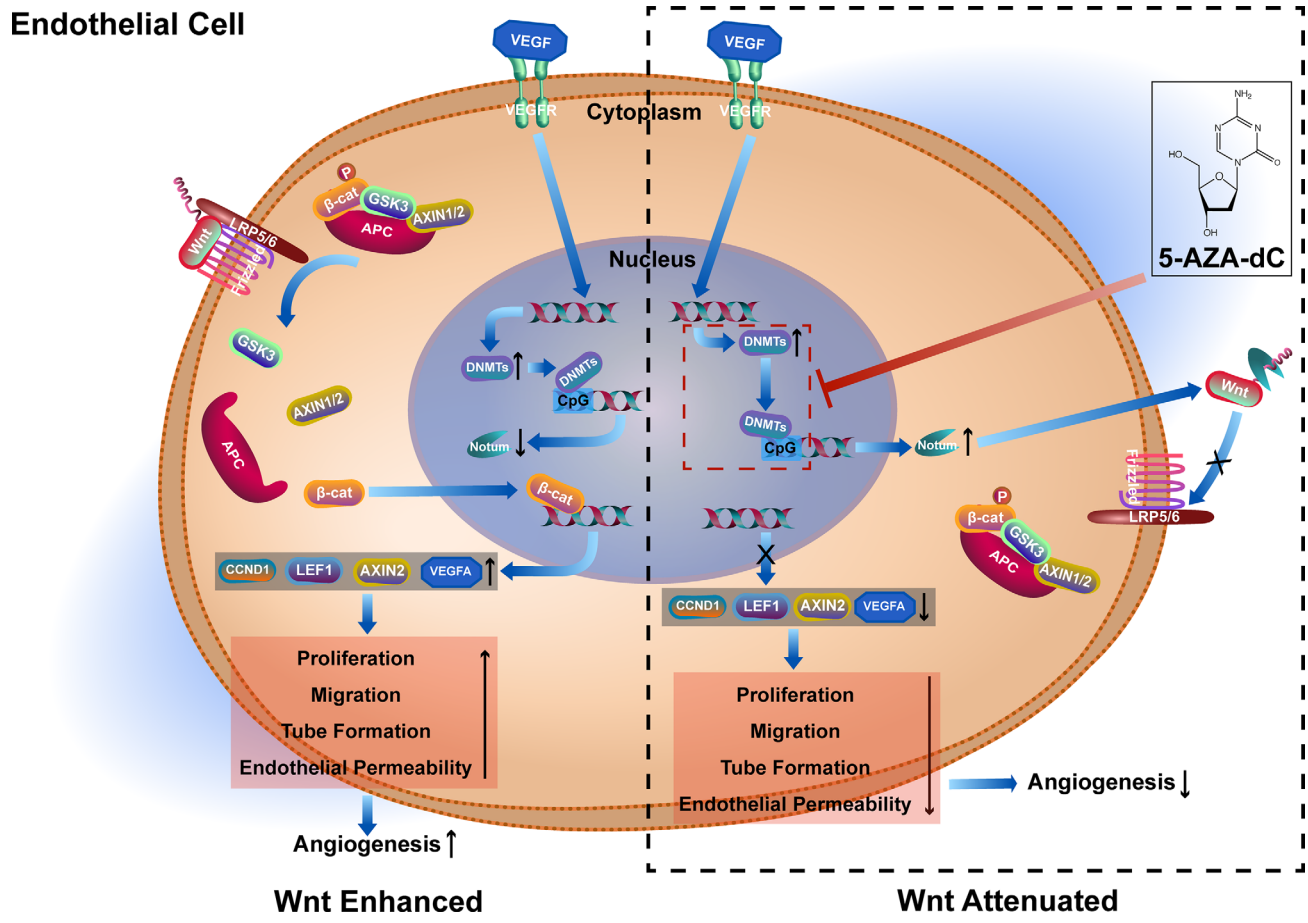


**Figure 6.** Schematic diagram depicting the mechanisms of 5-aza-dC treatment in inhibiting choroidal neovascularization in a laser-induced mouse model. During laser-induced CNV, VEGFA promotes expression of DNMTs and hypermethylation of the *Notum* promoter by binding to VEGF receptor in choroid/retinal endothelial cell. Because it is a Wnt antagonist, downregulation of *Notum* leads to Wnt pathway hyperactivation and subsequently endothelial cell proliferation, migration, and hyperpermeability (*left panel*). Inversely, 5-aza-dC administration reverses the effects of VEGFA on endothelial cell and inhibits CNV formation (*right panel*).

Investigative Ophthalmology & Visual Science

### *Acknowledgments*

Supported by grants from the National Nature Science Foundation of China (81970817, 81873680, 81800843) and the Natural Science Foundation of Xiamen (3502Z20227277).

Disclosure: **X. Wu**, None; **X. Yang**, None; **X. Dai**, None; **X. Chen**, None; **M. Shen**, None; **J. Dai**, None; **F. Yuan**, None; **L. Wang**, None; **Y. Yuan**, None; **Y. Feng**, None

### *References*

1. Grossniklaus HE, Green WR. Choroidal neovascularization. *Am J Ophthalmol*. 2004;137(3):496–503.
2. Kent D, Sheridan C. Choroidal neovascularization: a wound healing perspective. *Mol Vis*. 2003;9:747–755.
3. Cheung G, Lai T, Gomi F, Ruamviboonsuk P, Koh A, Lee WK. Anti-VEGF therapy for neovascular AMD and polypoidal choroidal vasculopathy. *Asia Pac J Ophthalmol (Phila)*. 2017;6(6):527–534.
4. Ohno-Matsui K, Ikuno Y, Lai T, Cheung CMG. Diagnosis and treatment guideline for myopic choroidal neovascularization due to pathologic myopia. *Prog Retin Eye Res*. 2018;63:92–106.
5. Campochiaro PA. Molecular pathogenesis of retinal and choroidal vascular diseases. *Prog Retin Eye Res*. 2015;49:67–81.
6. Mettu PS, Allingham MJ, Cousins SW. Incomplete response to anti-VEGF therapy in neovascular AMD: exploring disease mechanisms and therapeutic opportunities. *Prog Retin Eye Res*. 2021;82:100906.
7. Yang S, Zhao J, Sun X. Resistance to anti-VEGF therapy in neovascular age-related macular degeneration: a comprehensive review. *Drug Des Devel Ther*. 2016;10:1857–1867.
8. Solomon SD, Lindsley K, Vedula SS, Krzstolik MG, Hawkins BS. Anti-vascular endothelial growth factor for neovascular age-related macular degeneration. *Cochrane Database Syst Rev*. 2019;3(3):CD005139.
9. Ng D, Ho M, Iu L, Lai TYY. Safety review of anti-VEGF therapy in patients with myopic choroidal neovascularization. *Expert Opin Drug Saf*. 2022;21(1):43–54.
10. Moore LD, Le T, Fan G. DNA methylation and its basic function. *Neuropsychopharmacology*. 2013;38(1):23–38.
11. Mattei AL, Bailly N, Meissner A. DNA methylation: a historical perspective. *Trends Genet*. 2022;38(7):676–707.
12. Rasoulinejad SA, Maroufi F. A review of DNA and histone methylation alterations in the new era of diagnosis and treatment of retinal diseases. *Curr Mol Med*. 2021;21(8):607–619.
13. Wu J, Liu LL, Cao M, et al. DNA methylation plays important roles in retinal development and diseases. *Exp Eye Res*. 2021;211:108733.
14. Corso-Diaz X, Jaeger C, Chaitankar V, Swaroop A. Epigenetic control of gene regulation during development and disease: a view from the retina. *Prog Retin Eye Res*. 2018;65:1–27.
15. Dhillon S. Decitabine/cedazuridine: first approval. *Drugs*. 2020;80(13):1373–1378.
16. Zhou Z, Li HQ, Liu F. DNA methyltransferase inhibitors and their therapeutic potential. *Curr Top Med Chem*. 2018;18(28):2448–2457.
17. Christman JK. 5-Azacytidine and 5-aza-2′-deoxycytidine as inhibitors of DNA methylation: mechanistic studies and their implications for cancer therapy. *Oncogene*. 2002;21(35):5483–5495.
18. Xie MY, Yang Y, Liu P, Luo Y, Tang S-B. 5-aza-2′-deoxycytidine in the regulation of antioxidant enzymes in retinal endothelial cells and rat diabetic retina. *Int J Ophthalmol*. 2019;12(1):1–7.
19. Xie M, Tian J, Luo Y, Wei L, Lin S, Tang S. Effects of 5-aza-2′-deoxycytidine and trichostatin A on high glucose- and interleukin-1$\beta$-induced secretory mediators from human retinal endothelial cells and retinal pigment epithelial cells. *Mol Vis*. 2014;20:1411–1421.
20. He S, Barron E, Ishikawa K, et al. Inhibition of DNA methylation and methyl-CpG-binding protein 2 suppresses RPE transdifferentiation: relevance to proliferative vitreoretinopathy. *Invest Ophthalmol Vis Sci*. 2015;56(9):5579–5589.
21. Nashine S, Nesburn AB, Kuppermann BD, Kenney MC. Age-related macular degeneration (AMD) mitochondria modulate epigenetic mechanisms in retinal pigment epithelial cells. *Exp Eye Res*. 2019;189:107701.
22. Feng Y, Wang L, Dong C, et al. MicroRNA-376b-3p suppresses choroidal neovascularization by regulating glutaminolysis in endothelial cells. *Invest Ophthalmol Vis Sci*. 2023;64(1):22.
23. Feng Y, Zou R, Zhang X, et al. YAP promotes ocular neovascularization by modifying PFKFB3-driven endothelial glycolysis. *Angiogenesis*. 2021;24(3):489–504.
24. Meyer JH, Larsen PP, Strack C, et al. Optical coherence tomography angiography (OCT-A) in an animal model of laser-induced choroidal neovascularization. *Exp Eye Res*. 2019;184:162–171.
25. Park JR, Choi W, Hong HK, et al. Imaging laser-induced choroidal neovascularization in the rodent retina using optical coherence tomography angiography. *Invest Ophthalmol Vis Sci*. 2016;57(9):OCT331–OCT340.
26. Mizutani T, Ashikari M, Tokoro M, Nozaki M, Ogura Y. Suppression of laser-induced choroidal neovascularization by a CCR3 antagonist. *Invest Ophthalmol Vis Sci*. 2013;54(2):1564–1572.
27. Martinotti S, Ranzato E. Scratch wound healing assay. *Methods Mol Biol*. 2020;2109:225–229.
28. Watanabe T, Dohgu S, Takata F, et al. Paracellular barrier and tight junction protein expression in the immortalized brain endothelial cell lines bEND.3, bEND.5 and mouse brain endothelial cell 4. *Biol Pharm Bull*. 2013;36(3):492–495.
29. Kebir H, Kreymborg K, Ifergan I, et al. Human $T_H17$ lymphocytes promote blood-brain barrier disruption and central nervous system inflammation. *Nat Med*. 2007;13(10):1173–1175.
30. Orozco LD, Chen HH, Cox C, et al. Integration of eQTL and a single-cell atlas in the human eye identifies causal genes for age-related macular degeneration. *Cell Rep*. 2020;30(4):1246–1259.
31. Ritchie ME, Phipson B, Wu D, et al. limma powers differential expression analyses for RNA-sequencing and microarray studies. *Nucleic Acids Res*. 2015;43(7):e47.
32. Law CW, Chen Y, Shi W, Smyth GK. voom: precision weights unlock linear model analysis tools for RNA-seq read counts. *Genome Biol*. 2014;15(2):R29.
33. Voigt AP, Whitmore SS, Lessing ND, et al. Spectacle: an interactive resource for ocular single-cell RNA sequencing data analysis. *Exp Eye Res*. 2020;200:108204.
34. Voigt AP, Mullin NK, Mulfaul K, et al. Choroidal endothelial and macrophage gene expression in atrophic and neovascular macular degeneration. *Hum Mol Genet*. 2022;31(14):2406–2423.
35. Curradi M, Izzo A, Badaracco G, et al. Molecular mechanisms of gene silencing mediated by DNA methylation. *Mol Cell Biol*. 2002;22(9):3157–3173.
36. Hsieh CL. Dependence of transcriptional repression on CpG methylation density. *Mol Cell Biol*. 1994;14(8):5487–5494.
37. Lin JB, Sene A, Wiley LA, et al. Wnt7A/B promote choroidal neovascularization. *Exp Eye Res*. 2018;174:107–112.

38. Hu Y, Chen Y, Lin M, Lee K, Mott RA, Ma J. Pathogenic role of the Wnt signaling pathway activation in laser-induced choroidal neovascularization. *Invest Ophthalmol Vis Sci*. 2013;54(1):141–154.
39. Kakugawa S, Langton PF, Zebisch M, et al. Notum deacylates Wnt proteins to suppress signalling activity. *Nature*. 2015;519(7542):187–192.
40. Zhang X, Cheong SM, Amado NG, et al. Notum is required for neural and head induction via Wnt deacylation, oxidation, and inactivation. *Dev Cell*. 2015;32(6):719–730.
41. Wu SC, Zhang Y. Active DNA demethylation: many roads lead to Rome. *Nat Rev Mol Cell Biol*. 2010;11(9):607–620.
42. Hunter A, Spechler PA, Cwanger A, et al. DNA methylation is associated with altered gene expression in AMD. *Invest Ophthalmol Vis Sci*. 2012;53(4):2089–2105.
43. Oliver VF, Jaffe AE, Song J, et al. Differential DNA methylation identified in the blood and retina of AMD patients. *Epigenetics*. 2015;10(8):698–707.
44. Li Z, Li Y, Hou Y, et al. Association of plasma vitamins and carotenoids, DNA methylation of LCAT, and risk of age-related macular degeneration. *Nutrients*. 2023;15(13):2985.
45. Porter LF, Saptarshi N, Fang Y, et al. Whole-genome methylation profiling of the retinal pigment epithelium of individuals with age-related macular degeneration reveals differential methylation of the *SKI*, *GTF2H4*, and *TNXB* genes. *Clin Epigenetics*. 2019;11(1):6.
46. Berndsen RH, Abdul UK, Weiss A, et al. Epigenetic approach for angiostatic therapy: promising combinations for cancer treatment. *Angiogenesis*. 2017;20(2):245–267.
47. Hellebrekers DM, Jair KW, Vire E, et al. Angiostatic activity of DNA methyltransferase inhibitors. *Mol Cancer Ther*. 2006;5(2):467–475.
48. Lambert V, Lecomte J, Hansen S, et al. Laser-induced choroidal neovascularization model to study age-related macular degeneration in mice. *Nat Protoc*. 2013;8(11):2197–2211.
49. Maugeri A, Barchitta M, Fallico M, Castellino N, Reibaldi M, Agodi A. Characterization of SIRT1/DNMTs functions and LINE-1 methylation in patients with age-related macular degeneration. *J Clin Med*. 2019;8(2):159.
50. Liu Y, Tian X, Liu S, et al. DNA hypermethylation: a novel mechanism of CREG gene suppression and atherosclerogenic endothelial dysfunction. *Redox Biol*. 2020;32:101444.
51. Thangavel J, Malik AB, Elias HK, et al. Combinatorial therapy with acetylation and methylation modifiers attenuates lung vascular hyperpermeability in endotoxemia-induced mouse inflammatory lung injury. *Am J Pathol*. 2014;184(8):2237–2249.
52. Lindner DJ, Wu Y, Haney R, et al. Thrombospondin-1 expression in melanoma is blocked by methylation and targeted reversal by 5-Aza-deoxycytidine suppresses angiogenesis. *Matrix Biol*. 2013;32(2):123–132.
53. Clevers H, Nusse R. Wnt/$\beta$-catenin signaling and disease. *Cell*. 2012;149(6):1192–1205.
54. Shah R, Amador C, Chun ST, et al. Non-canonical Wnt signaling in the eye. *Prog Retin Eye Res*. 2023;95:101149.
55. Vallee A. Curcumin and Wnt/$\beta$–catenin signaling in exudative age–related macular degeneration (Review). *Int J Mol Med*. 2022;49(6):79.
56. Wang Z, Liu CH, Huang S, Chen J. Wnt signaling in vascular eye diseases. *Prog Retin Eye Res*. 2019;70:110–133.
57. Tuo J, Wang Y, Cheng R, et al. Wnt signaling in age-related macular degeneration: human macular tissue and mouse model. *J Transl Med*. 2015;13:330.
58. Hu Y, Chen Y, Lin M, Lee K, Mott RA, Ma J-x. Pathogenic role of the Wnt signaling pathway activation in laser-induced choroidal neovascularization. *Invest Ophthalmol Vis Sci*. 2013;54(1):141–154.
59. Shen M, Feng Y, Wang J, Yuan Y, Yuan F. CXCR7 inhibits fibrosis via Wnt/$\beta$-catenin pathways during the process of angiogenesis in human umbilical vein endothelial cells. *Biomed Res Int*. 2020;2020:1216926.


Investigative Ophthalmology & Visual Science